

# Effective Online 3D Bin Packing with Lookahead Parcels Using Monte Carlo Tree Search

Jiangyi Fang<sup>1,4</sup>, Bowen Zhou<sup>2</sup>, Haotian Wang<sup>3</sup>, Xin Zhu<sup>3</sup>, Leye Wang<sup>1,4\*</sup>

<sup>1</sup> Key Lab of High Confidence Software Technologies (Peking University), Ministry of Education, China

<sup>2</sup> Faculty of Computing, Harbin Institute of Technology, Harbin, China

<sup>3</sup> JD Logistic, Beijing, China

<sup>4</sup> School of Computer Science, Peking University, Beijing, China

fangjiangyi2001@gmail.com, leye wang@pku.edu.cn

## Abstract

Online 3D Bin Packing (3D-BP) with robotic arms is crucial for reducing transportation and labor costs in modern logistics. While Deep Reinforcement Learning (DRL) has shown strong performance, it often fails to adapt to real-world short-term distribution shifts, which arise as different batches of goods arrive sequentially, causing performance drops. We argue that the short-term lookahead information available in modern logistics systems is key to mitigating this issue, especially during distribution shifts. We formulate online 3D-BP with lookahead parcels as a Model Predictive Control (MPC) problem and adapt the Monte Carlo Tree Search (MCTS) framework to solve it. Our framework employs a dynamic exploration prior that automatically balances a learned RL policy and a robust random policy based on the lookahead characteristics. Additionally, we design an auxiliary reward to penalize long-term spatial waste from individual placements. Extensive experiments on real-world datasets show that our method consistently outperforms state-of-the-art baselines, achieving over 10% gains under distributional shifts, 4% average improvement in online deployment, and up to more than 8% in the best case—demonstrating the effectiveness of our framework.

## Keywords

3D Bin Packing, Reinforcement Learning, Model Predictive Control

## 1 Introduction

The global logistics market is anticipated to grow from 6.68 trillion to 11.27 trillion dollars in 2024 and 2033 with a growth rate of 5.98% according to the market report [31]. For logistics companies (e.g., JD Logistics [2] and Amazon [1]), bin packing represents a critical quality control measure within the supply chain. For example, improved space utilization of bin packing leads to substantial reductions in transportation costs [4]. However, due to the high labor costs and practical sequential constraints (e.g., placement

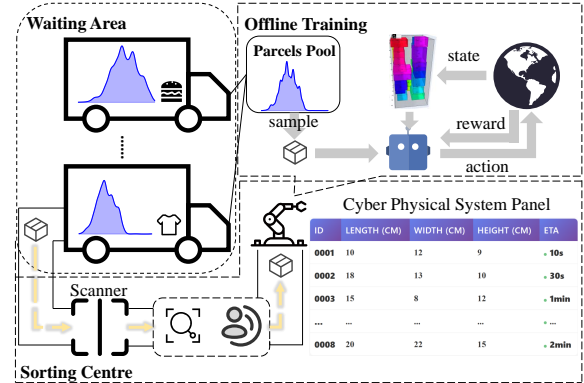


**Figure 1: The mismatch between the real-world online scenario and offline DRL training pipeline.**

decisions must be made one by one at once for parcels traveling on a conveyor belt to prevent their accumulation), researchers are increasingly turning their research focus to online 3D bin packing using robotic arms [42, 45]

Existing studies are primarily divided into heuristics [7, 8, 11, 13, 17, 25, 39, 41, 45, 47] and Deep Reinforcement Learning (DRL) methods [39, 44, 45, 47–49]. Heuristics rules are usually summarized from workers’ experience, e.g., layer first [40], deep bottom left first [18], corner first [20] etc. Although DRL has recently surpassed heuristics after extensive training, both approaches fail to address a real-world scenario with short-term distributional shifts. As shown in Figure 1, sorting centers with limited space must unload trucks sequentially in their arrival order. Since trucks carry parcels from different warehouses (e.g., food with varying sizes versus clothes with uniform sizes), this process creates a non-stationary parcel stream. However, current online DRL algorithms are trained on parcels sampled from a static pool [47, 48], which aggregates parcels from all warehouses and is updated at a fixed cycle (e.g., weekly). Consequently, they cannot adapt to such shifts in practice.

With progress in Cyber-Physical Systems and sensing technology [26, 32, 52], an online agent can acquire information about parcels as they pass through a scanner. As shown in Figure 1, information shown on the panel forms a lookahead queue: newly scanned parcels are appended to the end, while parcels successfully packed into a bin are removed from the front. This queue partially reveals the size distribution of upcoming parcels, allowing the agent to detect shifts and adjust its policy in advance.

However, it is challenging to utilize lookahead information to enhance the online policy both efficiently and effectively. One approach is to use planning-based methods [3, 15, 51] with sequential

\*Corresponding author.

Permission to make digital or hard copies of all or part of this work for personal or classroom use is granted without fee provided that copies are not made or distributed for profit or commercial advantage and that copies bear this notice and the full citation on the first page. Copyrights for components of this work owned by others than the author(s) must be honored. Abstracting with credit is permitted. To copy otherwise, or republish, to post on servers or to redistribute to lists, requires prior specific permission and/or a fee. Request permissions from permissions@acm.org.

Conference acronym 'XX, Woodstock, NY

© 2018 Copyright held by the owner/author(s). Publication rights licensed to ACM.

ACM ISBN 978-1-4503-XXXX-X/2018/06

https://doi.org/XXXXXXXX.XXXXXXX

decision constraints. Nonetheless, their efficiency is often insufficient for online applications due to the inherent computational complexity (*BFS* inference overhead over 100s shown in Table 2). Another straightforward method, encoding lookahead parcels as part of the state in DRL context, proved insufficient by our experiments (*PCT-lookahead* in Table 1) and existing works [47]. Furthermore, Zhao et al. proposed a reordering algorithm to condition the current parcel placement on subsequent ones [47]. However, these approaches miss the fundamental issue. Given that RL is already forward-looking by nature [21], these methods fail to question why this inherent foresight is insufficient in online 3D-BP. In fact, lookahead parcels may not always bring about improvement to the same degree in the context of 3D-BP. As shown in Figure 14 and Section 3, the greater the deviation of the short-term distribution from the original, the larger the potential performance gain from lookahead information.

When faced with unfamiliar parcels, human workers may unpack recently placed items [35, 45] to conduct several placement trials, evaluating the best option based on their historical experience. Inspired by this human intelligence, we formulate the online 3D-BP with lookahead parcels as a Model Predictive Control (MPC) problem [12, 19]. In this formulation, “placement trial” corresponds to a set of finite-horizon placement trajectories, while the “evaluation through historical experience” is achieved by using a well-trained online RL critic to select the optimal path. This mathematical formulation enables us to apply advanced techniques to tackle the problem. The main contributions of this paper are as follows:

- To the best of our knowledge, we are the first to establish that lookahead information is most valuable during short-term distributional shifts and to formulate the online 3D-BP with lookahead parcels as an MPC problem. Furthermore, we believe our approach could offer inspiration for other similar Markov Decision Process problems involving a finite lookahead horizon.
- We adapt the Monte Carlo Tree Search (MCTS) [37] framework to the 3D-BP scenario to solve the MPC problem formulated above. To adapt the MCTS exploration strategy for short-term shifts, we design a dynamic mechanism to adjust the exploration prior, balancing between a robust random policy and an offline-learned RL policy according to the likelihood of lookahead parcels appearing in the training dataset. Furthermore, to adapt the MCTS simulation and backup phases for the 3D-BP application, we introduce an auxiliary reward term that penalizes the wasted volume from each placement, considering its long-term effect on future parcels.
- We conduct extensive experiments on two real-world settings and an online evaluation, achieving over 10% improvements against state-of-the-art DRL baselines under distributional shifts, and about 4% average improvement in online deployment, validating the effectiveness of our proposed framework.

## 2 Problem Formulation

We will present our problem formulation in MDP form.

**State Space.** A state  $s_t \in S$  is a tuple  $s_t = (B_t, d_t)$ , where  $B_t$  can be represented by 2D height maps [47] or packing configuration tree [48] and  $d_t = (l_t, w_t, h_t)$  represents the length  $l_t$ , width  $w_t$  and height  $h_t$  of the parcel for step  $t$ .

**Action Space.** For a state  $s_t$ , the action space  $A_{s_t}$  is the set of all valid placements for the parcel  $d_t$ . A placement  $a_t = (x, y, z) \in A_{s_t}$  is a decision that maps to a specific position and orientation. Any valid action must satisfy all physical constraints (e.g., boundary, collision, stability).

**Transition Function.** The transition function  $P(s_{t+1}|s_t, a_t)$  has a hybrid nature. The next state  $s_{t+1} = (B_{t+1}, d_{t+1})$  has two parts. For the next bin state  $B_{t+1}$ , the state transition function is **deterministic**, which is denoted as  $B_{t+1} = f(B_t, d_t, a_t)$ . For the next parcel state  $d_{t+1}$ , the state transition function is **stochastic**:  $d_{t+1} \sim \mathcal{D}$ . In practice, we collect an offline dataset  $D$  to estimate the ideal distribution  $\mathcal{D}$ .

**Reward Function.** The immediate reward  $r_t = R(s_t, a_t)$  can be defined as the volume of the packed item (i.e.,  $l_t * w_t * h_t$ ) normalized by the total bin volume (i.e.,  $L * W * H$ ), encouraging space utilization.

**Online 3D-BP with Lookahead Parcels.** Our problem setting includes several known components: a lookahead sequence of  $N$  parcels (i.e.,  $d_t, d_{t+1}, \dots, d_{t+N-1}$  is known at step  $t$ ), an offline-trained DRL critic  $V_\theta$  and policy  $\pi_\theta$ , the offline dataset  $D$ , and a deterministic bin state transition function  $f$ . Given these components, our objective is to optimize the following function:

$$\max_{a_t, \dots, a_{t+N-1}} \mathbb{E} \left[ \sum_{k=0}^{N-1} (R(s_{t+k}, a_{t+k}) + V(s_{t+N})) \right] \quad (1)$$

where  $s_t = (B_t, d_t)$ ,  $B_{t+1} = f(B_t, d_t, a_t)$ , and  $d_{t+N} \sim D$ . We set the discount factor  $\gamma = 1$ , as each episode terminates in a finite number of steps (i.e., the bin becomes full). It is a typical MPC problem, allowing the agent to resist short-term distributional shifts by solving this optimization online. Following the receding horizon principle, once the optimal action trajectory is found, we execute only the first action  $a_t^*$  and then replan at the subsequent step  $t + 1$  with new lookahead parcels appended.

## 3 Theoretical Analysis

In this section, we first present the optimization objective for the conventional online 3D-BP problem and introduce the basic MDP formulation as it applies to this problem. We then theoretically derive the relationship between the magnitude of a distributional shift and the corresponding performance degradation of a previously optimal policy.

### 3.1 Preliminaries on online 3D-BP

Given the definition above, the goal of conventional online 3D-BP is to obtain an optimal policy  $\bar{\pi}(a|s)$  which satisfies the following equation:

$$\bar{\pi} = \arg \max_{\pi} \sum_{t=1}^{\infty} r_t \quad (2)$$

whose corresponding optimal value function,  $V_D^*(s)$ , uniquely satisfies the Bellman optimality equation for this stationary environment:

$$V_D^*(s_t) = \max_{a \in A} (R(s_t, a) + \gamma \sum_{s_{t+1} \in S} P(s_{t+1}|s_t, a) V_D^*(s_{t+1})) \quad (3)$$

Since the transition function stochastic part only contains  $d_{t+1} \sim D$ , the equation can be rewritten as:

$$V_D^*(s_t) = \max_{a \in A} (R(s_t, a_t) + \gamma \mathbb{E}_{d_{t+1} \sim D} [V_D^*(s_{t+1})]) \quad (4)$$

### 3.2 Failure in the non-stationary scenario.

Considering a realistic non-stationary distribution, the overall long-term distribution  $D$  is a mixture of these short-term distributions  $D_x$ :

$$D(d) = \sum_x D_x(d) \cdot P(X = x) \quad (5)$$

where  $X$  denotes a discrete random variable of the type of each batch of parcels.

For a determinate batch  $x$ , the value function  $V_{D_x}^{\bar{\pi}}$  in the new environment under policy  $\bar{\pi}$  is defined as follow:

$$V_{D_x}^{\bar{\pi}}(s_t) = \sum_{a_t \in A} \bar{\pi}(a_t | s_t) \left( R(s_t, a_t) + \gamma \mathbb{E}_{d_{t+1} \sim D_x} [V_{D_x}^{\bar{\pi}}(s_{t+1})] \right) \quad (6)$$

The optimal policy  $\pi^*$  under the distribution  $D_x$  is defined as follow:

$$V_{D_x}^*(s_t) = \max_{a_t \in A} \left( R(s_t, a_t) + \gamma \mathbb{E}_{d_{t+1} \sim D_x} [V_{D_x}^*(s_{t+1})] \right) \quad (7)$$

The performance gap between the optimal policy  $\pi^*$  and  $\bar{\pi}$  under the distribution  $D_x$  is defined as:

$$\text{Gap}(s) = V_{D_x}^*(s) - V_{D_x}^{\bar{\pi}}(s) \quad (8)$$

Actually, we can find that the performance gap can be bounded by the Total Variation distance between distributions.

$$|\text{Gap}(s)| \leq |V_{D_x}^*(s) - V_D^*(s)| + |V_{D_x}^*(s) - V_D^{\bar{\pi}}(s)| \leq C \cdot D_{TV}(D_x, D) \quad (9)$$

where  $D_{TV}(D_x, D)$  is the Total Variation distance [6, 28] between distributions and  $C$  is a constant (proof details can refer to Appendix A). As a result, a larger distance between the short-term distribution  $D_x$  and the long-term distribution  $D$  can lead to a proportionally larger drop in performance, which also implies larger potential improvement (i.e., considering lookahead parcels).

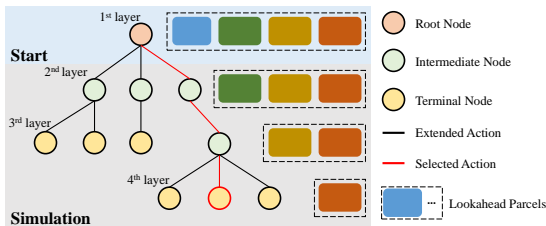


**Figure 2: Illustration for brute-force tree search solution for our MPC problem of online 3D-BP with lookahead parcels.**

## 4 Methodology

### 4.1 Tree Search Problem Modeling

The MPC problem above can be viewed as a tree search problem. Figure 2 illustrates how to solve this problem at a single decision step  $t$  using a brute-force search. The root node represents the initial state, comprising the current bin state  $B_t$  and the first parcel  $d_t$  from the lookahead queue. Starting from the root node (i.e., the 1<sup>st</sup> layer), we simulate all possible placement actions  $a \in A_{(B_t, d_t)}$  for the blue parcel. Each action, applied via the state transition function  $f$ , generates a new bin state  $B'$  in the next layer. The

edges in Figure 2 represent these state transitions. This process is repeated recursively; for instance, from each state in the second layer, we simulate placements for the green parcel to generate the third layer. The search terminates at a node (a terminal node) under two conditions: either the bin is full, or only one parcel remains in the lookahead sequence. In the latter case, we use the RL critic  $V(s)$  to estimate the value of the terminal state. After the tree is fully explored, we identify the trajectory leading to the terminal node with the highest value (highlighted in red) and select the first action on this path as the optimal choice. Thus, solving the MPC problem is equivalent to finding the optimal root-to-leaf path in this search tree. Although effective, this brute-force search is computationally infeasible due to its exponential complexity of  $O(|A|^N)$ . To address the inefficiency of brute-force search, we adapt the Monte Carlo Tree Search (MCTS) framework to the 3D-BP scenario to effectively balance exploration and exploitation. Our proposed *MPC-3D-BP* framework retains the standard phases of MCTS: *Selection*, *Expansion*, *Simulation*, and *Backup*. Our main technical contributions lie in two phases: first, an adapted exploration strategy for the *Selection* phase, and second, a novel penalty term for the value estimate used in the *Simulation and Backup* phase. Both MCTS and our *MPC-3D-BP* use the total number of trials  $n$  to control the search time budget.

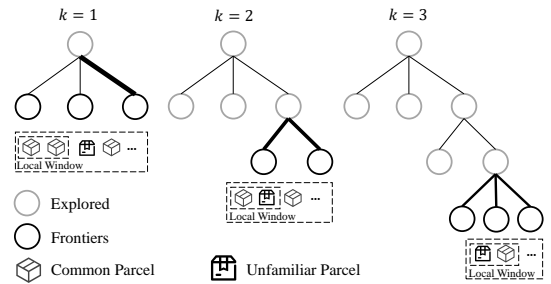


**Figure 3: Step by step illustration for how Shift-Aware Polynomial Upper Confidence Trees guide the selection. The thickness of edges represents the prior of action probability.**

### 4.2 MPC-3D-BP

#### 4.2.1 Selection with Shift-Aware Polynomial Upper Confidence Trees.

The goal of the *Selection* phase in MCTS is to traverse the existing tree from the root to a promising leaf node for expansion. This process must strike a balance between the exploitation of nodes known to have high value and the exploration of less-visited nodes that may have high potential.

State-of-the-art MCTS variants, such as those used in AlphaZero [33], employ the Polynomial Upper Confidence Trees (PUCT) algorithm for node selection. The action is chosen by maximizing:

$$a^* = \arg \max_a (Q(s, a) + c \cdot P_\pi(s, a) \cdot \frac{\sqrt{N(s)}}{1 + N(s, a)}) \quad (10)$$

Here,  $Q(s, a)$  is the exploitation term (mean action value), while the second term encourages exploration, guided by a prior probability  $P_\pi(s, a)$  from a learned policy network and a fixed exploration coefficient  $c$ .  $N(s)$  represents the total number of visits for node  $s$  and  $N(s, a)$  represents the number of visits for node  $s$ 's child node generated through action  $a$ .

A key limitation of the standard PUCT formulation is its reliance on the learned policy prior  $P_\pi(s, a)$  being equally reliable in all situations. This assumption is violated in our setting when a short-term distributional shift occurs. For a rare and unseen lookahead sequence  $I_{sub}$ , the learned prior  $P_\pi(s, a)$  can be misleading, yet the PUCT algorithm continues to trust it. This can trap the search in suboptimal regions suggested by an unreliable “intuition”.

To address this, we propose a novel mechanism that dynamically modulates the exploration prior based on the rarity of the current lookahead sequence. Instead of using the raw policy prior  $P_\pi(s, a)$ , we introduce a dynamic shift-aware prior,  $P_{SA}(a|s)$ , which performs a principled interpolation between trusting the learned policy and reverting to a robust, uniform exploration strategy.

The dynamic prior is defined as:

$$P_{SA}(a|s) = \alpha(s) \cdot P_\pi(s, a) + (1 - \alpha(s)) \cdot \frac{1}{|A_s|} \quad (11)$$

The interpolation weight  $\alpha(s) \in [0, 1]$  is the “Familiarity Score” of the local lookahead subsequence  $I_k$  at state  $s$ . The calculation of  $\alpha(s)$  is designed to be simple yet effective. The process is divided into two stages.

**Offline Pre-computation.** We process the entire training dataset  $D$  to build a probability look-up table for item types. First, we discretize the continuous item dimensions ( $l, w, h$ ) into a finite vocabulary of  $M$  unique item types using heuristics through visualization. Then, we compute the empirical probability  $P(\text{type}_j)$  for each item type by counting its frequency in the training data.

**Online Calculation.** During the MCTS search, for the given node  $s$  at the  $k^{\text{th}}$  layer of the tree, we calculate its Familiarity Score  $\alpha(s)$  as follows. We consider a fixed-size (empirically set to 3 for the pattern 2 normal parcels and 1 big one in Figure 8) local window of  $w$  items, starting from the current item to be placed in the node’s lookahead queue, denoted as  $I_k = (d_{t+k-1}, d_{t+k}, \dots, d_{t+k+w-1})$ . Assuming the occurrence of each item in this window is independent, the joint probability is the product of their probabilities, which are retrieved from our pre-computed table. The Familiarity Score is this joint probability:

$$\alpha(s) = P(I_k) = \prod_{i=1}^w P(\text{Disc}(d_{t+i+k-1})) \quad (12)$$

where  $\text{Disc}(d_{t+i+k-1})$  is the function that maps item  $d_{t+i+k-1}$  to its discrete type.

By substituting this dynamic prior into the PUCT formula, we get our final **Shift-Aware PUCT** selection rule:

$$a^* = \arg \max_a (Q(s, a) + c \cdot P_{SA}(a|s) \cdot \frac{\sqrt{N(s)}}{1 + N(s, a)}) \quad (13)$$

This formula exhibits intelligent, adaptive behavior, being aware of the rarity of the local lookahead sequence.

- **When the local lookahead sequence is common:** The prior term relatively approximates  $P_\pi(a|s)$ . As shown in the  $k = 1$  step in Figure 3, the algorithm trusts its learned intuition and efficiently exploits its knowledge, behaving like a standard PUCT (i.e., the distribution of actions with little uncertainty).
- **When a significant distributional shift occurs:** The prior term approximates the uniform distribution  $\frac{1}{|A_s|}$ . As shown in the  $k = 2, k = 3$  step in Figure 3, the algorithm recognizes that its

learned intuition is unreliable and gracefully degrades to a robust, non-informative exploration strategy, preventing the search from being led astray by a misleading prior.

This mechanism allows the search to dynamically allocate its exploration preference, investing more in broad exploration for novel challenges while efficiently leveraging learned knowledge for familiar situations.

**4.2.2 Expansion.** Once the *Selection* phase reaches a leaf node  $s_L$  that has not been expanded before, the *Expansion* phase is initiated to grow the search tree. To avoid the intractable cost of creating nodes for all possible actions, we follow state-of-the-art methods and use our learned policy network  $P_\pi(a|s)$  to guide this process.

For each valid action  $a \in A_{s_L}$ , we add a corresponding new child node to the tree. The edge leading from the parent node  $s_L$  to this new child is initialized with the following statistics:

- Visit Count:  $N(s_L, a) \leftarrow 0$
- Action Value:  $Q(s_L, a) \leftarrow 0$
- Prior Probability:  $P_{SA}(a|s) \leftarrow \alpha(s) \cdot P_\pi(s, a) + (1 - \alpha(s)) \cdot \frac{1}{|A_{s_L}|}$

After this step, the node  $s_L$  is now an internal node, and the search tree has been successfully expanded with new leaves ready for future selection and evaluation.

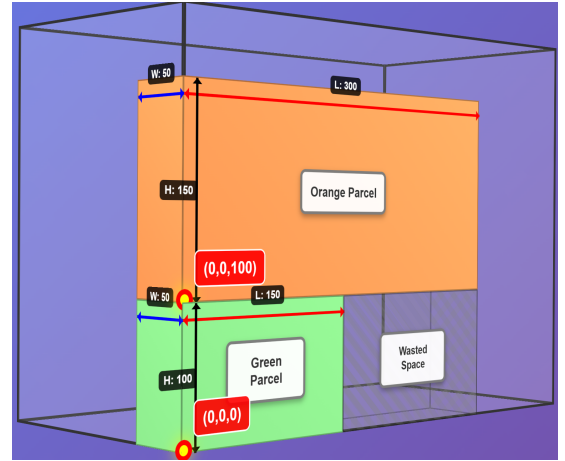


Figure 4: Illustration for waste space calculation.

**4.2.3 Simulation and Value Backup.** The *Simulation* phase in traditional MCTS involves performing a random or heuristic-based rollout from a newly expanded leaf node to the end of the game to obtain an estimate of its value. However, to improve efficiency, modern implementations like AlphaZero [33] often replace this costly rollout with a direct value estimate from a learned critic,  $V_\theta$ . In our MPC-based framework, the value of an entire  $N$ -step plan (a root-to-leaf path in the search tree) is similarly backed up. The standard approach is to sum the immediate rewards collected along the path and bootstrap the terminal value using the critic:

$$Q(a_t, a_{t+1}, \dots, a_{t+N-1}) = \sum_{k=0}^{N-1} r_{t+k} + V_\theta(s_{t+N}) \quad (14)$$

The rationale for explicitly summing the short-term rewards, rather than just relying on  $V_\theta(s_t)$ , is to ground the value estimate in the

factual outcomes of the known lookahead sequence, mitigating the potential unreliability of the critic when facing a short-term distributional shift.

However, this standard backup mechanism has a significant drawback in the context of 3D-BP. The standard reward signal,  $r_{t+k}$  (typically based on placed volume), is often insensitive in the early and middle stages of the packing process. Most valid placements yield similar, positive rewards, failing to differentiate a structurally efficient placement from one that catastrophically wastes space for future items. This places an enormous burden on the terminal value estimate  $V_\theta(s_{t+N})$ , which may not be robust enough to distinguish between states that have subtle but critical structural differences.

Therefore, inspired by the physical constraints of robotic packing, we propose a heuristic reward shaping scheme to create a more discerning, step-wise reward signal. Instead of only rewarding placed volume, we directly penalize the creation of wasted space along the short-term trajectory. In realistic scenarios, robotic arms can only place items from the top down due to gravity. Consequently, any space left underneath a newly placed item becomes practically inaccessible for all future placements and is effectively wasted. As shown in Figure 4, placing the orange parcel on top of the green one creates wasted space that is inaccessible to any future parcels.

To measure this, we introduce the **Wasted Space Penalty**. This penalty,  $R_p(s_k, a_k)$ , is calculated as the normalized volume of the space directly beneath the footprint of the item placed by action  $a_k$ . For example, in Figure 4, the wasted ratio is

$$\begin{aligned} R_p(s_k, a_k) &= (l_o * w_o - l_g * w_g) * (z_o - z_g) / (L * W * H) \\ &= (150 * 50 - 300 * 50) * (100 - 0) / (400 * 200 * 300) \\ &= 3.125\% \end{aligned} \quad (15)$$

where  $l_o, w_o, h_o$  are the dimensions of the orange parcel,  $l_g, w_g, h_g$  are the dimensions of the green one, and  $z_o, z_g$  are the placement coordinates of the orange and green parcels, respectively. This volume represents space that can no longer be utilized due to gravitational placement constraints. Our new shaped reward function,  $r'$ , incorporates this penalty:

$$r'_{t+k} = R_{\text{vol}}(s_k, a_k) - \lambda \cdot R_p(s_k, a_k) \quad (16)$$

where  $R_{\text{vol}}$  is the standard volume-based reward (e.g., the  $R_{\text{vol}}$  for orange parcel's placement in Figure 4 is calculated as  $\frac{l_o * w_o * h_o}{L * W * H} = \frac{300 * 50 * 150}{400 * 200 * 300} = 9.375\%$ ), and  $\lambda$  is a hyperparameter to adjust the weight of penalty term (we set  $\lambda = 0.5$  due to Figure 12).

The final value that is backed up through the MCTS tree, which we denote as  $Q'$ , uses this enriched reward signal:

$$Q'(a_t, a_{t+1}, \dots, a_{t+N-1}) = \sum_{k=0}^{N-1} r'_{t+k} + V_\theta(s_{t+N}) \quad (17)$$

After calculating the value  $Q'$ , the algorithm backs up this value along the selected trajectory, updating the  $Q(s, a)$  value for each node visited.

## 5 Offline Evaluation

### 5.1 Experiment Setup

**5.1.1 Datasets, baselines, and experiment settings.** We obtain the ground-truth parcel stream by mining historical logs and set the

lookahead number to  $N = 4$ , as this covers most online cases (see Figure 13 in Appendix B). To evaluate the effectiveness of our framework, we compare it against four heuristic methods (*LSAH* [13], *OnlineBPH* [11], *MACS* [14], *DBL* [18]) and two DRL methods (*PCT* [48], *GOPT* [44]) as baselines. Additionally, we implement two variants that incorporate lookahead information, *PCT-lookahead* and *PCT-reorder* [47]. To validate our specific technical contributions, we also conduct an ablation study with several alternative techniques (*BFS* [50], *Random* [29], *RTDP* [5], *MCTS* [33]). Additionally, we test the effectiveness of our framework under two settings **Realistic** and **Virtual**. We set up the **Virtual** setting following the setting in *PCT* [48], while the **Realistic** setting contains more real-world constraints on action space like collision avoidance. Details of datasets, baselines, and settings are provided in Appendix C.

**5.1.2 Evaluation metrics.** According to Zhao et al., we evaluate the performance of the 3D-BP algorithms using two core metrics [47]: space utilization (“Space Uti.”) and the number of packed items (“# Items”) (in Appendix C.3). To assess efficiency, we also record the average inference time per placement, denoted as “Infer. Time”. Furthermore, we define two evaluation scenarios: **Overall** and **Shift**. The **Overall** scenario computes these metrics across all test bins, whereas the **Shift** scenario calculates them exclusively for bins where the incoming parcel stream exhibits a significant distributional shift.

## 5.2 Results and Analysis

**5.2.1 Main Results.** In Table 1, we report the Space Uti., # Items and Infer. Time in both **Overall** and **Shift** scenarios under two settings. Table 1 shows that methods properly considering lookahead parcels (*PCT-reorder* and *MPC-PCT*) achieve better results than baselines, justifying the effectiveness of lookahead information. Specifically, *MPC-PCT* achieves over 15% improvement against *PCT* in the **Shift** scenario on both metrics, indicating that lookahead parcels are especially useful under distributional shifts. Besides, our *MPC-PCT* achieves notably better results than *PCT-reorder* and *PCT-lookahead* (over 10% improvement in the **Shift** scenario on both metrics), indicating our method of considering lookahead parcels reaching the state-of-the-art in practice. Besides, we also test our framework on another DRL baseline *GOPT* and obtain similar observations (*MPC-GOPT* and *MPC-PCT* obviously outperform the corresponding baselines with the green background color), which validates our framework’s generalization ability. Additionally, we can observe all results above under the **Virtual** setting, indicating our framework generalization across different action spaces (with different practical constraints). Although our framework achieves promising results, it takes about 3 times higher inference costs than *PCT-reorder* and over 10 times higher inference costs than *PCT*. However, it can meet the online requirements according to the detailed analysis in Section 6.

**5.2.2 Ablation study.** To better evaluate our technical contributions, we conduct an ablation study by implementing several alternative tree search techniques to solve our MPC problem. Table 2 displays the results under the Realistic setting. First, all tree search techniques outperform the baseline *PCT* in both scenarios, which validates the effectiveness of framing the problem within an MPC

**Table 1: Results on the same dataset for Realistic and Virtual settings. DRL baselines are colored with light green. The best two results are highlighted (*best* is in bold and *italic*, second-best is in bold).**

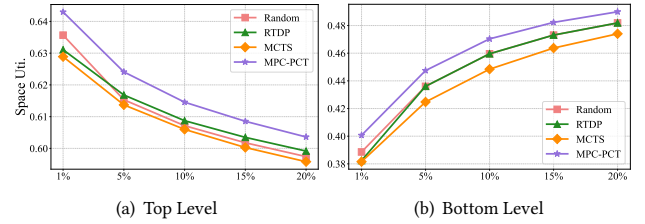
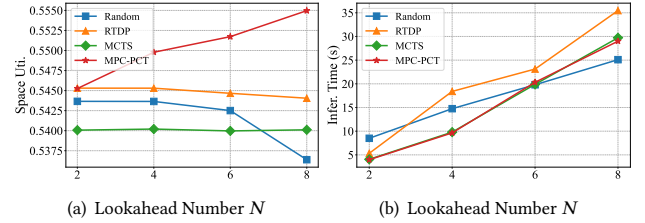
	Realistic					Virtual				
	Overall		Shift		Infer. Time	Overall		Shift		Infer. Time
	Space Util.	# Items	Space Util.	# Items		Space Util.	# Items	Space Util.	# Items	
<b>Baselines</b>										
<i>LSAH</i>	0.2396	15.29	0.2570	21.20	< 1s	0.2928	19.47	0.3218	23.64	< 1s
<i>OnlineBPH</i>	0.2903	18.50	0.3345	27.07	< 1s	0.3568	23.28	0.3700	26.83	< 1s
<i>MACS</i>	0.3826	24.41	0.3899	31.44	< 1s	0.4783	30.68	0.4668	32.86	< 1s
<i>DBL</i>	0.3677	23.56	0.4234	33.90	~ 5s	0.4379	28.37	0.4584	32.46	~ 5s
<i>PCT</i>	0.5395	34.14	0.4600	36.37	< 1s	0.5519	35.30	0.5227	36.47	< 1s
<i>GOPT</i>	0.5211	33.14	0.4461	36.06	< 1s	0.5331	34.27	0.5234	36.60	< 1s
<b>Lookahead Information Enhanced</b>										
<i>PCT-lookahead</i>	0.5286	33.41	0.4788	37.59	< 1s	0.5457	34.90	0.5428	37.63	< 1s
<i>PCT-reorder</i>	<b>0.5435</b>	<b>34.39</b>	0.4903	38.36	~ 3s	<b>0.5638</b>	<b>36.01</b>	0.5651	38.98	~ 3s
<b>Ours</b>										
<i>MPC-PCT</i>	<b>0.5498</b>	<b>34.80</b>	<b>0.5258</b>	<b>40.61</b>	~ 10s	<b>0.5765</b>	<b>36.83</b>	<b>0.6034</b>	<b>41.45</b>	~ 10s
<i>MPC-GOPT</i>	0.5403	34.31	<b>0.5165</b>	<b>40.10</b>	~ 20s	0.5527	35.48	<b>0.5927</b>	<b>40.70</b>	~ 20s

**Table 2: Ablation study results under the Realistic setting. The best two results excluding *BFS* are highlighted (*best* is in bold and *italic*, second-best is in bold).**

	Realistic				
	Overall		Shift		Infer. Time
	Space Util.	# Items	Space Util.	# Items	
<b>Alternative Techniques</b>					
<i>BFS</i>	0.5513	34.91	0.5403	41.71	~ 100s
<i>Random</i>	0.5436	34.42	0.4955	38.75	~ 15s
<i>RTDP</i>	0.5453	34.50	0.4956	38.54	~ 18s
<i>MCTS</i>	0.5402	34.19	0.4679	37.03	~ 10s
<b>Ours</b>					
~ w/o <i>WSP</i>	<b>0.5494</b>	<b>34.77</b>	<b>0.5218</b>	<b>40.32</b>	~ 10s
~ w/o <i>SAPUCT</i>	0.5410	34.25	0.4723	37.41	~ 10s
<i>MPC-PCT</i>	<b>0.5498</b>	<b>34.80</b>	<b>0.5258</b>	<b>40.61</b>	~ 10s

framework. Second, while brute-force search (*BFS*) achieves the best performance, its inference overhead is approximately 10 times higher than that of the other techniques, making it impractical. Additionally, *RTDP* with its  $\epsilon$ -greedy strategy performs more robustly than the pure exploration of the *Random* baseline in the **Overall** scenario. However, a standard *MCTS* with Polynomial Upper Confidence Trees relies too heavily on the prior DRL policy, resulting in limited performance gains. Notably, removing our proposed exploration strategy (~ w/o *SAPUCT*) causes a significant performance drop, particularly in the **Shift** scenario (an 11.3% reduction in space utilization). This result underscores the importance of a well-designed strategy that balances the DRL prior with random exploration. Similarly, the underperformance of the variant without our waste space penalty (~ w/o *WSP*) confirms the effectiveness of this proposed term.

**5.2.3 Robustness analysis at different levels.** To evaluate the robustness of *MPC-PCT*, we analyze its performance on subsets of

**Figure 5: Performance comparison under different levels.****Figure 6: Scalability**

bins ranked by final space utilization, specifically the top and bottom {1%, 5%, 10%, 15%, 20%}. Figure 5 plots the space utilization for each performance rank. We observe that *MPC-PCT* (purple line) consistently achieves the highest space utilization across all levels, demonstrating its robustness. Among the baselines, *RTDP* (green line) outperforms the *Random* policy (pink line) in the median percentiles but underperforms at the extremes. This suggests that while an  $\epsilon$ -greedy exploration strategy may be effective for typical cases, a pure exploration approach can be more beneficial in the most extreme (easiest or hardest) scenarios.

**5.2.4 Analysis of scalability.** To analyze the scalability of *MPC-PCT* and other search techniques, we conduct experiments by varying the lookahead horizon *N*. The results are presented in Figure 6. We observe that only the performance of *MPC-PCT* improves consistently as *N* increases. Notably, the performance of the pure random exploration strategy (*Random*, blue line) degrades dramatically

with a larger  $N$ , eventually becoming worse than the baseline  $PCT$  (which uses no lookahead). Furthermore, the performance of  $MCTS$  and  $RTDP$  remains largely unchanged as  $N$  increases. This suggests that a proper balance between exploration and exploitation is crucial to effectively leverage a larger lookahead horizon. Additionally, the inference time of  $MPC-PCT$  scales nearly linearly with  $N$ , which is consistent with its theoretical computational complexity of  $O(nN)$ .

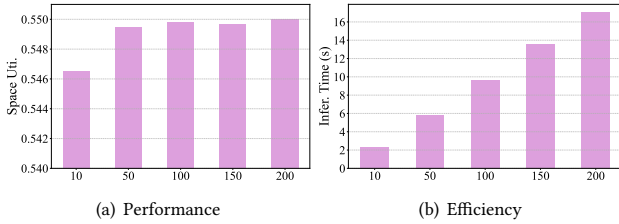


Figure 7: The number of trials  $n$  sensitivity.

5.2.5 *Effect of number of trials  $n$ .* Figure 7 shows the Space Utilization and Inference Time of  $MPC-PCT$  as a function of  $n$  (the total number of trials), while the lookahead horizon  $N$  is held constant. We observe two key trends: (i) as  $n$  increases, the Space Utilization improves and eventually plateaus; and (ii) the Inference Time increases linearly with  $n$ . Therefore, in practice, a trade-off can be made to achieve a sufficiently effective policy within a limited time budget. For instance, when  $N = 4$ , setting  $n = 100$  yields near-optimal results in approximately 10 seconds.

### 5.3 Case Study

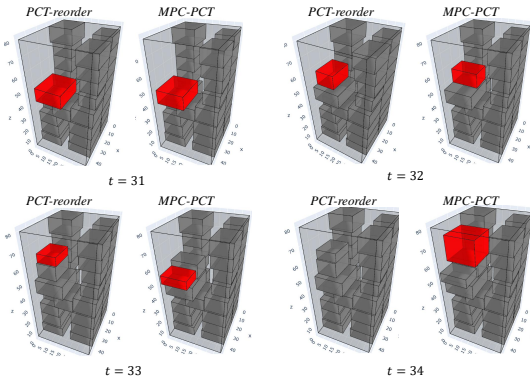


Figure 8: Case study on  $PCT-reorder$  and  $MPC-PCT$ . The red parcel is the current parcel to be packed at step  $t$ . If there is no red parcel means the bin is full.

We visualize the bin packing results for  $PCT-reorder$  and  $MPC-PCT$  on an identical sequence of parcels. For a clear and fair comparison, we use the baseline  $PCT$  policy to pack all parcels before step  $t = 31$ , ensuring both algorithms begin with the same bin state. As shown in Figure 8, the incoming sequence from  $t = 31$  to  $t = 34$  consists of two extremely large parcels and two normally-sized ones.  $PCT-reorder$  fails to pack the final parcel at  $t = 34$  because it still fundamentally relies on the learned  $PCT$  policy and cannot sufficiently alter its behavior for this difficult sequence. In contrast,

$MPC-PCT$  successfully packs the final parcel by adjusting its policy in advance; it rotates the parcels at  $t = 32$  and  $t = 33$  to create the necessary space for the item at  $t = 34$ . This demonstrates our framework’s ability to solve complex cases that simpler lookahead methods like  $PCT-reorder$  cannot.

## 6 Online Deployment

To validate the practical utility and real-world performance of our framework, we partnered with JD Logistics to deploy our framework in their intelligent bin packing system (Appendix C.5).



Figure 9: Engineering adjustment for system efficiency. Time interval for two consecutive parcels’ arrival can be controlled to 15 seconds.

### 6.1 Engineering Adjustment

To deploy  $MPC-3D-BP$  framework in the online robotic arm bin packing system, we first combine the well-trained production baseline model into our framework. Besides, we also try to optimize the efficiency at both the system level and the algorithm level. For system level, as shown in the original part of Figure 9, the existing online system treats calculation (i.e., grasp point generation, placement point generation, and trajectory generation) and robotic arm execution as separate, sequential processes, leading to a tight time budget for calculation to prevent parcel accumulation. However, as shown in the optimized part of Figure 9, robotic arm execution for the last parcel and calculation for the current parcel can run in parallel. This optimization can save at most about 10 seconds (i.e., extended time budget in Figure 9) for placement point generation (i.e., Online 3D-BP algorithm), where  $T_p = \min(T_a, T_e) - T_t - T_g \approx 12s - 1s - 10ms \approx 11s, T_a$  for average time interval for consecutive parcels’ arrival,  $T_e$  for average time for robotic arm execution,  $T_t$  for average time for trajectory generation,  $T_g$  for average time for grasp point generation. For the algorithm level, we change the terminal condition for our algorithm from the number of trials to running time. In addition, since the current lookahead queue and the next lookahead queue have  $N - 1$  overlapped parcels, we cache the best child and the corresponding subtree of the root node to initialize the MCTS tree when the next parcel arrives.

### 6.2 A/B Test Results

We conduct online A/B tests on four parallel robotic arm lines, two of them equipped with the online 3D-BP DRL model (production baseline), and another two of them equipped with our proposed



Figure 10: Real-world cases for our intelligent 3D-BP system with robotic arms.

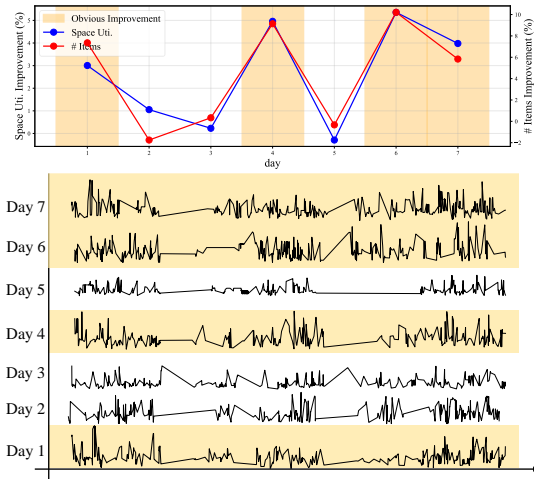


Figure 11: Online deployment results for 7 days.

method. The results of the week-long online A/B test are presented in Figure 11. Our method achieves an average of 2.6% higher space utilization and 4.4% higher number of packed parcels compared to the production baseline.

To understand why our model performs better on certain days (1, 4, 6, and 7, highlighted in orange), we analyze the corresponding parcel volume streams. The bottom of Figure 11 plots the volume of the parcel (i.e.,  $l * w * h$ ) over a week, revealing distinct batches arriving throughout each day (e.g., morning, afternoon). The key observation is that the days with the largest performance gains coincide with the most volatile parcel streams (i.e., about 966  $\text{cm}^3$  alve of standard deviation<sup>1</sup>), whereas days with minimal improvement have more stable and consistent volumes (i.e., about 705  $\text{cm}^3$  standard deviation). Generally, we apply our methods in 3 sorting centers with 20 robotic arms. Since 2025-07 till now, we have already processed over 100000 parcels and packed over 2000 bins. Example real-world bin packing cases are shown in Figure 10.

## 7 Related Work

Studies on the online 3D-BP problem generally fall into two categories: heuristic-based and DRL-based methods. Heuristic approaches codify human-designed strategies into rules, such as maximizing available space [3, 43]. Some offline heuristics can be directly applied in online settings [3]. Representative methods include OnlineBPH [11], which introduces the Empty Maximal Spaces (EMS) heuristic prioritizing large empty regions; Walle [39], which incorporates wall-building and layer-building strategies. In contrast, DRL-based methods learn placement policies through interaction

<sup>1</sup>We calculate the standard deviation for 30 parcels as a window and average the standard deviation for all windows to obtain the final result

with simulated environments. PackMan [39] was among the first to apply DRL in online 3D-BP. Zhao et al. [47] introduced a feasibility mask to model the task as a constrained MDP, while Zhao et al. [49] proposed a Packing Configuration Tree (PCT) to guide DRL in continuous action spaces. AR2L [27] designed a permutation-based attacker to maintain DRL performance under nominal and adversarial scenarios. GOPT [44] employed a transformer to better capture spatial relations between parcels and the bin. Additionally, several studies enhance performance by enabling repacking actions inspired by human strategies [30, 35, 38, 45]. Lookahead information is pivotal in many sequential decision-making problems, such as Model Predictive Control (MPC) and Markov Decision Processes (MDPs) [19, 22, 23]. In MDPs, numerous algorithms combine planning and RL to leverage lookahead, often refining base RL policy during training via search or optimization [9, 10, 24, 34]. Alternatively, MPC-based methods solve a planning problem online at each step to achieve improved decision quality [12].

## 8 Conclusion

In this paper, we present *MPC-3D-BP*, an online optimization framework based on Monte Carlo Tree Search for the online 3D-BP with lookahead parcels problem, designed to address the short-term distributional shifts common in real-world scenarios. To effectively balance exploration and exploitation, we propose a novel exploration strategy that is aware of potentially unfamiliar parcels in the lookahead queue. Additionally, we introduce a step-wise penalty to the reward function that penalizes wasted space, thereby accounting for the long-term impact of each placement. We conduct extensive experiments on datasets from both realistic and virtual settings. The results demonstrate that *MPC-3D-BP* outperforms baselines that lack lookahead capabilities, and does so consistently when integrated with different underlying DRL models. Furthermore, we compare our framework against alternative problem formulations and MPC solution techniques, showing that our method achieves superior performance with an inference overhead that remains acceptable for online applications. Moreover, a week-long online A/B test on the live robotic packing system at JD Logistics confirms that *MPC-3D-BP* outperforms the production baseline, verifying its real-world effectiveness. As one of the first studies on online 3D-BP with lookahead parcels, we hope our research can benefit the development of intelligent packing systems and offer insights for other similar problems involving finite lookahead horizons.

## References

- [1] 2025. *Amazon*. <https://www.amazon.com> Accessed on July 18, 2025.
- [2] 2025. *JD Logistics*. <https://www.jdl.com> Accessed on July 18, 2025.
- [3] Sara Ali, António Galvão Ramos, Maria Antónia Carravilla, and José Fernando Oliveira. 2022. On-line three-dimensional packing problems: A review of off-line

- and on-line solution approaches. *Computers & Industrial Engineering* 168 (2022), 108122.
- [4] Mauro Maria Baldi, Daniele Manerba, Guido Perboli, and Roberto Tadei. 2019. A generalized bin packing problem for parcel delivery in last-mile logistics. *European Journal of Operational Research* 274, 3 (2019), 990–999.
  - [5] Andrew G Barto, Steven J Bradtke, and Satinder P Singh. 1995. Learning to act using real-time dynamic programming. *Artificial intelligence* 72, 1-2 (1995), 81–138.
  - [6] Arnab Bhattacharyya, Sutanu Gayen, Kuldeep S Meel, Dimitrios Myrasiotis, Aduri Pavan, and NV Vinodchandran. 2022. On approximating total variation distance. *arXiv preprint arXiv:2206.07209* (2022).
  - [7] Bernard Chazelle. 1983. The Bottom-Left Bin-Packing Heuristic: An Efficient Implementation. *IEEE Trans. Comput.* (1983).
  - [8] Teodor Gabriel Crainic, Guido Perboli, and Roberto Tadei. 2008. Extreme Point-Based Heuristics for Three-Dimensional Bin Packing. *INFORMS Journal on Computing* (2008).
  - [9] Yonathan Efroni, Gal Dalal, Bruno Scherrer, and Shie Mannor. 2019. How to combine tree-search methods in reinforcement learning. In *Proceedings of the AAAI Conference on Artificial Intelligence*, Vol. 33. 3494–3501.
  - [10] Yonathan Efroni, Mohammad Ghavamzadeh, and Shie Mannor. 2020. Online planning with lookahead policies. *Advances in Neural Information Processing Systems* 33 (2020), 14024–14033.
  - [11] Chi Trung Ha, Trung Thanh Nguyen, Lam Thu Bui, and Ran Wang. 2017. An Online Packing Heuristic for the Three-Dimensional Container Loading Problem in Dynamic Environments and the Physical Internet. In *Applications of Evolutionary Computation*.
  - [12] Nicklas Hansen, Xiaolong Wang, and Hao Su. 2022. Temporal difference learning for model predictive control. *arXiv preprint arXiv:2203.04955* (2022).
  - [13] Haoyuan Hu, Xiaodong Zhang, Xiaowei Yan, Longfei Wang, and Yinghui Xu. 2017. Solving a new 3D bin packing problem with deep reinforcement learning method. *arXiv preprint arXiv:1708.05930* (2017).
  - [14] Ruizhen Hu, Juzhan Xu, Bin Chen, Minglun Gong, Hao Zhang, and Hui Huang. 2020. TAP-Net: transport-and-pack using reinforcement learning. *ACM Transactions on Graphics* (2020).
  - [15] Meng-Yu Huang, Ling-Ying Huang, Yu-Xing Zhong, Hui-Wen Yang, Xiao-Meng Chen, Wei Huo, Jia-Zheng Wang, Fan Zhang, Bo Bai, and Ling Shi. 2025. MILP acceleration: A survey from perspectives of simplex Initialization and learning-based branch and bound. *Journal of the operations research society of china* 13, 1 (2025), 1–55.
  - [16] Peiyuan Jiang, Daji Ergu, Fangyao Liu, Ying Cai, and Bo Ma. 2022. A Review of Korf algorithm developments. *Procedia computer science* 199 (2022), 1066–1073.
  - [17] Korhan Karabulut and Mustafa Murat Inceoglu. 2004. A hybrid genetic algorithm for packing in 3D with deepest bottom left with fill method. In *International Conference on Advances in Information Systems*. Springer, 441–450.
  - [18] Korhan Karabulut and Mustafa Murat Inceoglu. 2004. A Hybrid Genetic Algorithm for Packing in 3D with Deepest Bottom Left with Fill Method. In *Advances in Information Systems*.
  - [19] Basil Kouvaritakis and Mark Cannon. 2016. Model predictive control. *Switzerland: Springer International Publishing* 38, 13-56 (2016), 7.
  - [20] Silvano Martello, David Pisinger, and Daniele Vigo. 2000. The three-dimensional bin packing problem. *Operations research* 48, 2 (2000), 256–267.
  - [21] Yutaka Matsuo, Yann LeCun, Maneesh Sahani, Doina Precup, David Silver, Masashi Sugiyama, Eiji Uchibe, and Jun Morimoto. 2022. Deep learning, reinforcement learning, and world models. *Neural Networks* 152 (2022), 267–275.
  - [22] Nadav Merlis. 2024. Reinforcement Learning with Lookahead Information. *arXiv preprint arXiv:2406.02258* (2024).
  - [23] Nadav Merlis, Dorian Baudry, and Vianney Perchet. 2024. The value of reward lookahead in reinforcement learning. *Advances in Neural Information Processing Systems* 37 (2024), 83627–83664.
  - [24] Thomas M Moerland, Anna Deichler, Simone Baldi, Joost Broekens, and Catholijn M Jonker. 2020. Think too fast nor too slow: The computational trade-off between planning and reinforcement learning. *arXiv preprint arXiv:2005.07404* (2020).
  - [25] Ankush Ojha, Marichi Agarwal, Aniruddha Singhal, Chayan Sarkar, Supratim Ghosh, and Rajesh Sinha. 2021. A generalized algorithm and framework for online 3-dimensional bin packing in an automated sorting center. In *2021 Seventh Indian Control Conference (ICC)*. IEEE, 135–140.
  - [26] Sascha Julian Oks, Max Jalowski, Michael Lechner, Stefan Mirschberger, Marion Merklein, Birgit Vogel-Heuser, and Kathrin M Möslein. 2024. Cyber-physical systems in the context of industry 4.0: A review, categorization and outlook. *Information Systems Frontiers* 26, 5 (2024), 1731–1772.
  - [27] Yuxin Pan, Yize Chen, and Fangzhen Lin. 2023. Adjustable robust reinforcement learning for online 3D bin packing. *Advances in Neural Information Processing Systems* (2023).
  - [28] Kishan Panaganti, Zaiyan Xu, Dileep Kalathil, and Mohammad Ghavamzadeh. 2022. Robust reinforcement learning using offline data. *Advances in neural information processing systems* 35 (2022), 32211–32224.
  - [29] Robin Pemantle and Yuval Peres. 1995. Critical random walk in random environment on trees. *The Annals of Probability* (1995), 105–140.
  - [30] Aaron Valero Puche and Sukhan Lee. 2022. Online 3D bin packing reinforcement learning solution with buffer. In *IEEE/RSJ International Conference on Intelligent Robots and Systems*.
  - [31] Research and Markets. 2025. *Logistics Market - Trends, Innovations & Forecast 2025-2033*. <https://www.researchandmarkets.com/reports/6101938> Accessed on June, 2025.
  - [32] Hong SHAO, Daxiong XIE, and Yihua HUANG. 2021. A survey of intelligent sensing technologies in autonomous driving. *ZTE Communications* 19, 3 (2021), 56.
  - [33] David Silver, Thomas Hubert, Julian Schrittwieser, Ioannis Antonoglou, Matthew Lai, Arthur Guez, Marc Lanctot, Laurent Sifre, Dhharshan Kumaran, Thore Graepel, et al. 2018. A general reinforcement learning algorithm that masters chess, shogi, and Go through self-play. *Science* 362, 6419 (2018), 1140–1144.
  - [34] David Silver, Julian Schrittwieser, Karen Simonyan, Ioannis Antonoglou, Aja Huang, Arthur Guez, Thomas Hubert, Lucas Baker, Matthew Lai, Adrian Bolton, Yutian Chen, Timothy P. Lillicrap, Fan Hui, Laurent Sifre, George van den Driessche, Thore Graepel, and Demis Hassabis. 2017. Mastering the game of go without human knowledge. *Nature* (2017).
  - [35] Shuai Song, Shuo Yang, Ran Song, Shilei Chu, Wei Zhang, et al. 2023. Towards online 3d bin packing: Learning synergies between packing and unpacking via drl. In *Conference on Robot Learning*. PMLR, 1136–1145.
  - [36] Balakumar Sundaralingam, Siva Kumar Sastry Hari, Adam Fishman, Caelan Garrett, Karl Van Wyk, Valts Blukis, Alexander Millane, Helen Oleynikova, Ankur Handa, Fabio Ramos, et al. 2023. Curobo: Parallelized collision-free robot motion generation. In *2023 IEEE International Conference on Robotics and Automation (ICRA)*. IEEE, 8112–8119.
  - [37] Maciej Świechowski, Konrad Godlewski, Bartosz Sawicki, and Jacek Mańdziuk. 2023. Monte Carlo tree search: A review of recent modifications and applications. *Artificial Intelligence Review* 56, 3 (2023), 2497–2562.
  - [38] YP Tsang, DY Mo, KT Chung, and CKM Lee. 2025. A deep reinforcement learning approach for online and concurrent 3D bin packing optimisation with bin replacement strategies. *Computers in Industry* 164 (2025), 104202.
  - [39] Richa Verma, Aniruddha Singhal, Harshad Khadilkar, Ansuma Basumatary, Siddharth Nayak, Harsh Vardhan Singh, Swagat Kumar, and Rajesh Sinha. 2020. A generalized reinforcement learning algorithm for online 3d bin-packing. *arXiv preprint arXiv:2007.00463* (2020).
  - [40] Richa Verma, Aniruddha Singhal, Harshad Khadilkar, Ansuma Basumatary, Siddharth Nayak, Harsh Vardhan Singh, Swagat Kumar, and Rajesh Sinha. 2020. A generalized reinforcement learning algorithm for online 3D bin-packing. *arXiv preprint arXiv:2007.00463* (2020).
  - [41] Fan Wang and Kris Hauser. 2019. Stable Bin Packing of Non-convex 3D Objects with a Robot Manipulator. In *International Conference on Robotics and Automation*.
  - [42] Fan Wang and Kris Hauser. 2021. Dense robotic packing of irregular and novel 3D objects. *IEEE Transactions on Robotics* (2021).
  - [43] Wenjie Wu, Changjun Fan, Jincai Huang, Zhong Liu, and Junchi Yan. 2023. Machine learning for the multi-dimensional bin packing problem: Literature review and empirical evaluation. *arXiv preprint arXiv:2312.08103* (2023).
  - [44] Heng Xiong, Changrong Guo, Jian Peng, Kai Ding, Wenjie Chen, Xuchong Qiu, Long Bai, and Jianfeng Xu. 2024. GOPT: Generalizable online 3D bin packing via transformer-based deep reinforcement learning. *IEEE Robotics and Automation Letters* (2024).
  - [45] Shuo Yang, Shuai Song, Shilei Chu, Ran Song, Jiyu Cheng, Yibin Li, and Wei Zhang. 2023. Heuristics integrated deep reinforcement learning for online 3D bin packing. *IEEE Transactions on Automation Science and Engineering* (2023).
  - [46] Junpeng YU and Yiyu CHEN. 2023. A practical reinforcement learning framework for automatic radar detection. *ZTE Communications* 21, 3 (2023), 22.
  - [47] Hang Zhao, Qijin She, Chenyang Zhu, Yin Yang, and Kai Xu. 2021. Online 3D bin packing with constrained deep reinforcement learning. In *Proceedings of the AAAI Conference on Artificial Intelligence*, Vol. 35. 741–749.
  - [48] Hang Zhao, Yang Yu, and Kai Xu. 2022. Learning Efficient Online 3D Bin Packing on Packing Configuration Trees. In *International Conference on Learning Representations*.
  - [49] Hang Zhao, Chenyang Zhu, Xin Xu, Hui Huang, and Kai Xu. 2022. Learning practically feasible policies for online 3D bin packing. *Science China Information Sciences* (2022).
  - [50] Rong Zhou and Eric A Hansen. 2006. Breadth-first heuristic search. *Artificial Intelligence* 170, 4-5 (2006), 385–408.
  - [51] Qianwen Zhu, Xihan Li, Zihan Zhang, Zhixing Luo, Xialiang Tong, Mingxuan Yuan, and Jia Zeng. 2021. Learning to pack: A data-driven tree search algorithm for large-scale 3d bin packing problem. In *Proceedings of the 30th ACM International Conference on Information & Knowledge Management*. 4393–4402.
  - [52] Zhuo Zou, Qing Chen, Ismail Uysal, and Lirong Zheng. 2014. Radio frequency identification enabled wireless sensing for intelligent food logistics. *Philosophical Transactions of the Royal Society A: Mathematical, Physical and Engineering Sciences* 372, 2017 (2014), 20130313.

## A Proof Details

To quantify the suboptimality of the conventional policy  $\bar{\pi}$  in a non-stationary environment, we will derive a bound on the performance gap. This bound will show that the loss in performance is directly related to the statistical distance between the long-term average distribution  $D$  and the current short-term distribution  $D_x$ . We begin with a key lemma that bounds the change in the value of any fixed policy when the underlying environment distribution shifts from  $D$  to  $D_x$ .

**Lemma 1.** Let  $\pi$  be any fixed policy. Let  $V_D^\pi(s)$  and  $V_{D_x}^\pi(s)$  be the state-value functions of executing  $\pi$  in environments governed by distributions  $D$  and  $D_x$ , respectively. Assuming rewards are bounded in  $[0, R_{max}]$  (in 3D-BP scenario, rewards corresponding to space utilization are in  $[0, 1)$ ), the maximum difference between these value functions is bounded as follows:

$$\max_s |V_D^\pi(s) - V_{D_x}^\pi(s)| \leq \frac{\gamma R_{max}}{(1-\gamma)^2} \cdot D_{TV}(D, D_x) \quad (18)$$

where  $D_{TV}(D, D_x)$  is the Total Variation distance between the two distributions.

**Proof.**

Let  $\delta(s) = V_D^\pi(s) - V_{D_x}^\pi(s)$ . By the Bellman evaluation equation for a fixed policy  $\pi$ :

$$\delta(s) = (R(s, \pi(s)) + \gamma \mathbb{E}_{d' \sim D} [V_D^\pi(s')]) - (R(s, \pi(s)) + \gamma \mathbb{E}_{d' \sim D_x} [V_{D_x}^\pi(s')]) \quad (19)$$

$$\delta(s) = \gamma (\mathbb{E}_{d' \sim D} [V_D^\pi(s')] - \mathbb{E}_{d' \sim D_x} [V_{D_x}^\pi(s')]) \quad (20)$$

We add and subtract the term  $\gamma \mathbb{E}_{d' \sim D} [V_D^\pi(s')]$  inside the absolute value:

$$|\delta(s)| = \gamma \left| (\mathbb{E}_{d' \sim D} [V_D^\pi(s')] - \mathbb{E}_{d' \sim D_x} [V_D^\pi(s')]) + (\mathbb{E}_{d' \sim D_x} [V_D^\pi(s')] - \mathbb{E}_{d' \sim D_x} [V_{D_x}^\pi(s')]) \right| \quad (21)$$

$$|\delta(s)| \leq \gamma |\mathbb{E}_{d' \sim D} [V_D^\pi(s')] - \mathbb{E}_{d' \sim D_x} [V_D^\pi(s')]| + \gamma |\mathbb{E}_{d' \sim D_x} [V_D^\pi(s')] - \mathbb{E}_{d' \sim D_x} [V_{D_x}^\pi(s')]| \quad (22)$$

The value of any policy is bounded by  $V_{max} = \frac{R_{max}}{1-\gamma}$ . The difference between the expectations of a bounded function  $f$  under two distributions is bounded by  $2\|f\|_\infty D_{TV}$ . Applying this to the first term:

$$|\delta(s)| \leq \gamma \left( 2 \cdot \frac{R_{max}}{1-\gamma} \cdot D_{TV}(D, D_x) \right) + \gamma \mathbb{E}_{d' \sim D_x} [|\delta(s')|] \quad (23)$$

Let  $\|\delta\|_\infty = \max_s |\delta(s)|$ . Taking the maximum over all states  $s$ :

$$\begin{aligned} \|\delta\|_\infty &\leq \frac{2\gamma R_{max}}{1-\gamma} D_{TV}(D, D_x) + \gamma \|\delta\|_\infty \\ (1-\gamma) \|\delta\|_\infty &\leq \frac{2\gamma R_{max}}{1-\gamma} D_{TV}(D, D_x) \end{aligned} \quad (24)$$

This yields the bound (a slightly different constant due to the bounding technique, but the principle holds):

$$\|\delta\|_\infty \leq \frac{2\gamma R_{max}}{(1-\gamma)^2} D_{TV}(D, D_x) \quad (25)$$

This lemma formalizes that a small change in distribution leads to a proportionally small change in the value of any given policy. With this lemma, we can now prove our main theorem.

**Theorem 2 (Performance Gap Bound).** The performance gap of the conventional policy  $\bar{\pi}$  in an environment governed by  $D_x$  is bounded by a function of the statistical distance  $D_{TV}(D, D_x)$ .

**Proof.** The performance gap at a state  $s$  is defined as the difference between the true optimal value in the  $D_x$  environment and the value achieved by our conventional policy  $\bar{\pi}$  in that same environment:

$$\text{Gap}(s) = V_{D_x}^*(s) - V_{D_x}^{\bar{\pi}}(s) \quad (26)$$

We know that the policy  $\bar{\pi}$  is optimal for the stationary distribution  $Q$ . Therefore, its value function is the optimal one in that environment:  $V_D^{\bar{\pi}}(s) = V_D^*(s)$ .

We can rewrite the gap by adding and subtracting the value of the optimal policy for the stationary world,  $V_D^*(s)$ :

$$\text{Gap}(s) = (V_{D_x}^*(s) - V_D^*(s)) + (V_D^*(s) - V_{D_x}^{\bar{\pi}}(s)) \quad (27)$$

Substituting  $V_D^*(s) = V_D^{\bar{\pi}}(s)$ :

$$\begin{aligned} \text{Gap}(s) = & \underbrace{(V_{D_x}^*(s) - V_D^*(s))}_{\text{Term 1: Inherent Optimality Difference}} + \\ & \underbrace{(V_D^{\bar{\pi}}(s) - V_{D_x}^{\bar{\pi}}(s))}_{\text{Term 2: Policy Performance Degradation}} \end{aligned} \quad (28)$$

This decomposition is insightful. It shows that the total performance gap comes from two sources:

- (1) **Term 1:** The difference between the best possible performance in the new environment  $V_{D_x}^*$  versus the old environment  $V_D^*$ . This reflects how the environment's change inherently affects the optimal achievable value.
- (2) **Term 2:** The degradation in performance of our specific, fixed policy  $\bar{\pi}$

Using **Lemma 1**, we can directly bound Term 2:

$$|V_D^{\bar{\pi}}(s) - V_{D_x}^{\bar{\pi}}(s)| \leq \frac{2\gamma R_{max}}{(1-\gamma)^2} D_{TV}(D, D_x) \quad (29)$$

A similar, though more involved, proof based on the properties of the Bellman optimality operator as a contraction mapping can show that Term 1 is also bounded by the distribution distance:

$$|V_{D_x}^*(s) - V_D^*(s)| \leq \frac{2\gamma R_{max}}{(1-\gamma)^2} D_{TV}(D, D_x) \quad (30)$$

By applying the triangle inequality, the total performance gap is thus bounded:

$$|\text{Gap}(s)| \leq |V_{D_x}^*(s) - V_D^*(s)| + |V_D^{\bar{\pi}}(s) - V_{D_x}^{\bar{\pi}}(s)| \leq C \cdot D_{TV}(D, D_x) \quad (31)$$

where  $C = \frac{4\gamma R_{max}}{(1-\gamma)^2}$  is a constant.

Besides, the proof is already applicable to MDPs that can end in finite horizons where  $\gamma$  is often set to 1. Although it may seem that when  $\gamma = 1$ , the constant  $C$  goes to  $\infty$ , in fact, if the game can end in a maximum of  $T$  finite steps, the value of any policy is still bounded by  $T \cdot R_{max}$ . Other proof details remain unchanged.

## B Data Evidence and Additional Experiment Results

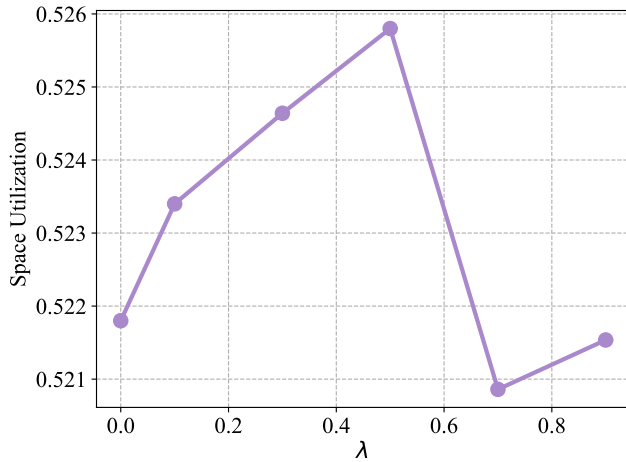


Figure 12: Parameters sensitivity study on waste space penalty  $\lambda$  in the Shift scenario.

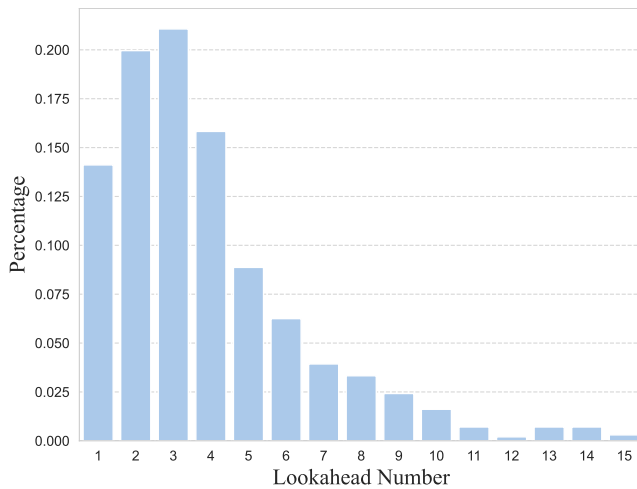


Figure 13: Common lookahead number  $N$  in Cyber-Physical System.

## C Implementation Details

### C.1 Dataset Preprocess and Statistics

The **offline training dataset** is mined from the historical robotic arm log in JD Logistics. We collect the length, width, and height of the parcels (detailed statistics in Table 3), as well as their grasp points, to serve as training inputs. All data are obtained under consistent real-world production conditions. The inclusion of grasp points as input features during training is determined by the specific experimental settings.

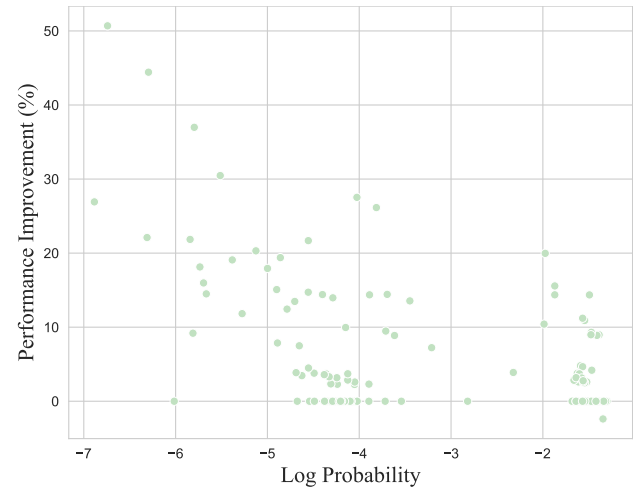


Figure 14: The log probability of online parcel batches, calculated relative to the offline training dataset, plotted against the corresponding performance gap between the *BFS* and *PCT* methods.

The **lookahead parcels dataset** is also created by mining historical robotic arm logs from JD Logistics. The raw logs contain detailed records for each parcel, including its dimensions (length, width, and height), arrival time, and the corresponding robotic arm actions (e.g., grasp points and placement coordinates). We extract this essential information and then sort the records by their arrival times to reconstruct the original parcel stream. To generate the lookahead information for each record, we first set a lookahead horizon  $N$ . Then, for each placement decision, its lookahead queue is formed by taking the next  $N - 1$  parcels from the sorted stream. The total number of records for the lookahead parcels dataset is 882.

Table 3: Dataset Statistics of offline training dataset.

Time Span	# Records	Length Range	Width Range	Height Range	Bin Size
2025.05-2025.06	5652	16 ~ 58	12 ~ 40	4 ~ 48	(94,80,160)

### C.2 Baselines

Heuristic methods are important baselines in the Online 3D-BP problem.

- *LSAH* [13]: According to Hu et al., a heuristic algorithm which goes over all empty maximal spaces and 2 orientations for the current item and chooses the empty maximal space and orientation that yields the least surface area when putting an item.
- *OnlineBPH* [11]: According to Ha et al., a heuristic algorithm which finds the first suitable placement within the allowed empty maximal spaces and orientations. All the empty maximal spaces are sorted with deep-bottom-left order.
- *MACS* [14]: According to Hu et al., a heuristic algorithm which calculates the best-scored position by the policy of maximizing remaining empty spaces. Candidate locations are generated from

the four corners of every empty maximal space under two possible orientations.

- *DBL* [17]: According to Karabulut and İnceoğlu, a heuristic algorithm which selects positions based on the Deepest Bottom Left with Fill (DBLF) policy, which prioritizes the deepest available slot, followed by the lowest, and then the leftmost position.

Besides, we implement two methods considering lookahead information:

- *PCT-lookahead*: a DRL method that encodes lookahead parcels as part of states.
- *PCT-reorder*: Following the work of Zhao et al., we implement a reordering algorithm that conditions the current placement decision on upcoming parcels. This method virtually reorders the sequence to place lookahead items first, while adhering to a critical order-dependence constraint: an earlier-arriving parcel cannot occupy a space made available only by the placement of a later-arriving one.

In addition, we choose two DRL methods as our backbone, where *PCT* is our main backbone and we also test our method’s effectiveness on *GOPT*.

- *PCT* is a state-of-the-art DRL model for online 3D-BP problem. It, through its novel tree-based representation, cleverly combines heuristic rules and deep reinforcement learning using the Graph Attention Network (GAT) [46] to solve the core challenge of an overly complex action space in the online 3D Bin Packing problem.
- *GOPT* is a state-of-the-art DRL model for online 3D-BP problem. It, through its unique "Generator-Transformer" architecture, achieves high performance and strong generalization for the 3D bin packing task, addressing the problem where traditional DRL methods often struggle to adapt to different environmental configurations.

To validate the effectiveness of our adaptation, we also implement many alternative general techniques to solve the same MPC problem.

- *BFS* [50]: We implement a brute-force search that traverses every possible root-to-leaf path to identify and select the optimal one.
- *Random* [29]: We implement many random walks on the tree where, for each path traversal, the algorithm starts at the root and randomly selects a child node to visit at each step until a leaf node is reached. After performing a predefined number of searches, we select the optimal path found among all explored trajectories.
- *RTDP* [5]: According to Barto et al., we implement a real-time dynamic programming algorithm in the context of the online 3D-BP problem.
- *MCTS* [33]: According to Silver et al., we adapt the MCTS framework used in AlphaZero directly to the 3D-BP environment.

### C.3 Metrics

The space utilization (Space Uti.) is calculated as follows:

$$\text{space\_utilization} = \frac{\sum_{i=1}^M l_i * w_i * h_i}{L * W * H} \quad (32)$$

where  $M$  is the number of parcels for the bin,  $L, W, H$  are the length, width, and height for the bin, respectively,  $l_i, w_i, h_i$  is the length, width, and height for the  $i^{th}$  parcel, respectively.

The number of parcels (# Items) is directly defined by its literal meaning.

### C.4 Experiment Settings

*Training*. In the offline training stage, we train two models: *PCT* and *GOPT*. For *PCT* training, we use the Empty Maximal Spaces (EMS) method to generate the action space and encode the state using a single graph attention layer. The hyperparameters for both deep models are fine-tuned via grid search. Key architectural parameters include an input embedding dimension of 64, a hidden layer dimension of 128, an internal node length of 120, and a leaf node length of 80. Additionally, the hyperparameters for the learning process are as follows: the learning rate is set to  $1 \times 10^{-6}$ , and the coefficients for both the actor and critic losses are set to 1.0. For *GOPT* training, we use EMS as the action space and encode the state using three transformer layers. When the model selects an EMS as the output, the parcel is placed at the deepest, lowest, and leftmost feasible position within the selected EMS. Key architectural parameters include an input embedding dimension of 128, an EMS length of 80. Additionally, the hyperparameters for the learning process are as follows: the learning rate is set to  $7 \times 10^{-5}$  at first with a linearly descending learning rate, and the coefficients for policy update and critic loss are respectively set to 0.96 and 0.5.

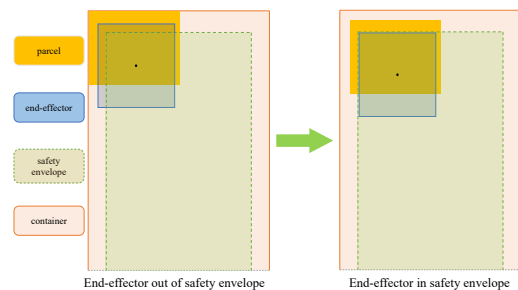


Figure 15: Top view of the position safety offset method.

*Testing*. We test two settings of the same dataset, **Realistic** and **Virtual**.

- **Virtual**. To comprehensively evaluate the performance of all methods on the parcel stream dataset, we use a sliding-window technique to generate short-term test batches that simulate the online scenario. Specifically, we set the window size to 100, which corresponds to the maximum number of items historically packed into a single bin, and generate these batches using a stride of 1. To evaluate a given method, we run it on each batch and then calculate the final performance by averaging the metrics across all resulting packed bins. Besides, we follow *Setting 1* in *PCT* [48]. Only two horizontal orientations are permitted, and the stability of the bin state is checked when the current parcel is placed.
- **Realistic**. With the same evaluation protocol of **Virtual** setting, we consider more practical constraints working with robotic arms. In the **Realistic** setting, the data includes the grasp point information of the robotic arm when picking up parcels, which is used to ensure operational safety in real-world scenarios. Given the constraints and limitations characteristic of real-world production

environments, the robotic arm's end-effector is at risk of colliding with the cage walls or previously placed parcels during item pick-and-place operations. To mitigate this risk, we define a safety zone—referred to as the safety envelope—within the cage, as illustrated in the figure 15, where the end-effector is only allowed to operate within the green area. Based on the upstream-provided grasp points, we calculate whether the current placement position would cause the end-effector to exceed the permissible range. Notably, when the parcel size is very small, the planned position may result in the end-effector exceeding the safety zone, rendering many placements infeasible. To address this issue, we designed a position safety offset method that computes the minimally offset placement position while still satisfying the safety requirements (Figure 15). This offsetting approach applies to all action generation schemes as well as heuristic methods. We apply this method in all realistic settings to ensure that the methods used perform reliably in real-world scenarios.

For a fair comparison, all DRL models were trained on a Linux server with 92 CPU cores (Intel® Xeon® Platinum 8468V), 922 GB of RAM, and a single NVIDIA GeForce RTX 4090D GPU. All methods were subsequently tested on a Linux server with 32 CPU cores and 120 GB of RAM.

## C.5 Deployment System



Figure 16: The scanner to upload parcel information onto the Cyber Physical System.



Figure 17: The overview of online 3D-BP with robotic arms.

The intelligent online 3D-BP system at JD Logistics can process at least 1500 parcels per robotic arm daily, reducing labor costs by the equivalent of approximately one full-time worker per robotic arm. The system consists of a scanner to obtain parcel information and a conveyor system for routing. As shown in Figure 16, the scanner reads a parcel's barcode from any face as it passes through. This information is then uploaded to the Cyber-Physical System, which determines the parcel's destination route. When the parcel reaches the end of the conveyor belt (Figure 17), a top-down camera captures an image and transmits it to the system. Our system uses a YOLO-based model [16] to detect the parcel in the image and calculates some suitable grasp points. Additionally, the server determines the optimal placement location by feeding the current bin state to an online DRL-based 3D-BP model. Finally, the central server computes a collision-free trajectory from the initial position of parcels to the target placement using CuRobo [36], avoiding the bin walls and other packed parcels.

Received 20 February 2007; revised 12 March 2009; accepted 5 June 2009